Numerical study of two phase laminar mixed convection nanofluid in elliptic ducts

Mohammad Shariat, Alireza Akbarinia, Alireza Hossein Nezhad, Rainer Laur

Accepted Manuscript

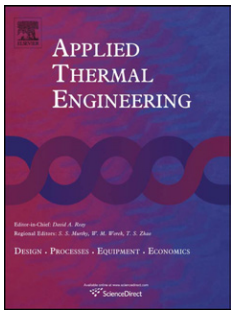

Title: Numerical study of two phase laminar mixed convection nanofluid in elliptic ducts

Authors: Mohammad Shariat, Alireza Akbarinia, Alireza Hossein Nezhad, Rainer Laur

PII: S1359-4311(11)00167-0

DOI: 10.1016/j.applthermaleng.2011.03.035

Reference: ATE 3490

To appear in: *Applied Thermal Engineering*

Received Date: 14 October 2010

Revised Date: 23 March 2011

Accepted Date: 26 March 2011

Please cite this article as: M. Shariat, A. Akbarinia, A.H. Nezhad, R. Laur. Numerical study of two phase laminar mixed convection nanofluid in elliptic ducts, Applied Thermal Engineering (2011), doi: 10.1016/j.applthermaleng.2011.03.035

Numerical study of two phase laminar mixed convection nanofluid in elliptic ducts

Mohammad Shariat[1], Alireza Akbarinia[2,*], Alireza Hossein Nezhad[1], Rainer Laur[2]

[1]Department of Mechanical Engineering, University of Sistan and Baluchestan, P.O. Box 98164-161 Zahedan, Iran.

[2] Institute for Electromagnetic Theory and Microelectronics (ITEM), University of Bremen, Germany

[*]Corresponding author
Tel: +49 421 2184438
Fax: +49 421 2184434
E-mail: a.akbarinia@item.uni-bremen.de

Abstract:

Laminar mixed convection Al_2O_3-Water nanofluid flow in elliptic ducts with constant heat flux boundary condition has been simulated employing two phase mixture model. Three-dimensional Navier-Stokes, energy and volume fraction equations have been discretized using the finite volume method. The Brownian motions of nanoparticles have been considered to determine the thermal conductivity and dynamic viscosity of Al_2O_3-Water nanofluid, which depend on temperature. Simulation effects of solid volume fraction, aspect ratio and buoyancy forced on thermal and hydraulics behaviors of nanofluid flow in elliptic ducts have been presented and discussed. The calculated results show good agreement with the previous numerical data. Results show that in a given Reynolds number (Re) and Richardson number (Ri), increasing solid nanoparticles volume fraction increases the Nusselt number (Nu) while the skin friction factor decreases. Increasing aspect ratio ($AR=b/a$) in elliptic tubes reduces the local skin friction factor whereas it does not have any specified effect on the local Nusselt number.

Keywords: Nanofluid, Mixed Convection, Two Phase, Elliptic Duct, Mixture Model.

Nomenclature

AR aspect ratio (=b/a)

a horizontal ellipse semi-axis (m)

a^* acceleration (ms^{-2})

b vertical ellipse semi-axis (m)

C_p specific heat (J kg^{-1} K^{-1})

D_h hydraulic diameter of tube (m)

d_f diameter of water molecular (m)

d_p diameter of nanoparticles (m)

f Fanning friction coefficient, ($= \tau_w \Big/ \left(\frac{1}{2}\rho_m u_i^2\right)$)

g gravitational acceleration (ms^{-2})

Gr Grashof number ($=\frac{g\beta_m q'' D_h^4}{k_m \upsilon_m^2}$)

k thermal conductivity (Wm^{-1} K^{-1})

k_B Boltzmann constant (=1.3807×10^{-23} J K^{-1})

L length of duct (m)

Nu local Nusselt number ($=\frac{q'' D_h}{k_m(T_w - T_b)}$)

P pressure (Pa)

Pr Prandtl number ($=\frac{\alpha_m}{\nu_m}$)

q'' uniform heat flux (Wm^{-2})

Re Reynolds number ($=\frac{\rho_m u_i D_h}{\mu_m}$)

Ri Richardson number ($=\frac{Gr}{\mathrm{Re}^2}$)

T temperature (K)

V velocity (ms^{-1})

x, y, z coordinates

X dimensionless horizontal semi-axis ($=\frac{x}{a}$)

Y dimensionless vertical semi-axis ($=\frac{y}{b}$)

Z non-dimensional length ($=\frac{z}{D_h}$)

Greek Letters

α thermal diffusivity($=\frac{\mu_m}{\rho_m}$)

β volumetric expansion coefficient (K^{-1})

δ distance between particles (m), which define in Eq. (15)

ϕ nanoparticles volume fraction

η variable, defined in Eq. (21)

λ_f mean free path of water molecular (m)

μ dynamic viscosity (N s m^{-2})

ν kinematic viscosity (m^2 s^{-1})

θ dimensionless temperature ($=\frac{T-T_i}{(q'' D_h)/k_m}$)

ρ density (kg m^{-3})

τ_w shear stress at the wall

Subscripts

b bulk

dr drift

f base fluid

k indices

i inlet conditions

m mixture

p particle and solid phase

w wall

1. Introduction

Nanofluid is a suspension of nanoparticles such as Al_2O_3, *Cu* or *CuO* in a base fluid such as water, ethylene glycol, or oil. Nanofluids have attracted enormous interest from researchers due to high thermal conductivity and their potential for high rate of heat exchange incurring either little or no penalty in pressure drop. It has been found that the thermal conductivity of nanofluids is notably higher than that of the base fluid. Many attempts in this field have been made to formulate appropriate effective thermal conductivity and dynamic viscosity of nanofluid [1-6]. Das et al. [7] and Putra et al. [8] have investigated a water–Al_2O_3 mixture experimentally and found that increasing temperature increases the effective thermal conductivity remarkably while the dynamic viscosity decreases. It has been shown that the thermal conductivity of nanofluids increases with increasing temperature [9-11]. Yu et al. [11] measured that the thermal conductivity of *ZnO-EG* nanofluid. They found that the enhanced value of 5.0 vol. % *ZnO-EG* nanofluid is 26.5%, well beyond the values given by the existing classical models for the solid–liquid mixture, and is consistent with the prediction values by the combination of the aggregation mechanism with the Maxwell and Bruggeman models. Teng et al. [12] have measured the effects of temperature, nanoparticles size and weight fraction on the thermal conductivity of Al_2O_3-Water nanofluid. They compared their results

with numerical results and proposed a good correlation for thermal conductivity, which depends on temperature, nanoparticles size and weight fraction. Murshed et al. [13] have done a similar experimental work, which has been considered the effects of particle size, nanolayer, Brownian motion, and particle surface chemistry and interaction potential on the thermal conductivity of nanofluids, and proposed a new model for thermal conductivilty.

The two phases or single phase approach could be applied for simulating convective heat transfer with nanofluids. The single phase approach is simpler and requires less computational time, which assumes that the fluid phase and particles are in thermal equilibrium and move with the same velocity. But using appropriate expressions which calculate the properties of single phase nanofluid are important and notable. However, the single phase approach has been used in several theoretical studies of convective heat transfer with nanofluids [14-23]. Hence the properties of nanofluids are not completely specified and there are not good expressions for predicting nanofluid mixture, generally the single phase numerical prediction are not in good agreement with experimental results.

On the other hand, several factors such as gravity, friction between the fluid and solid particles and Brownian forces, the phenomena of Brownian diffusion, sedimentation, and dispersion may affect a nanofluid flow. Consequently, the slip velocity between the fluid and particles must be take into account for simulating nanofluid flows [1]. Since the two phase approach considers the movement between the solid and fluid molecular, it has better prediction in nanofluid fluid study. To fully describe and predict the flow and behavior of complex flows, different multiphase theories have been proposed and used. The large number of published articles concerning multiphase flows typically employed the Mixture Theory or the theory of interacting continua [24-27]. This approach is based on the underlying assumption that each phase can be mathematically described as a continuum. Lotfi et al. [28] simulated nanofluids flow in a horizontal circular tube with three different approaches, which

are a single phase model, two phase Mixture model and two phase Eulerian model. They found by comparison with experimental results, that the two phase mixture model is more precise than the other two models. Some researcher have employed two phase Mixture theory to predict the behavior of nanofluids [29-32]. Akbarinia and Laur [30] and Mirmasoumi and Behzadmehr [32] studied the effect of nanoparticles diameter on nanofluid fluid in horizontal curved tubes with circular cross section.

The tubes of elliptic cross section have drawn special attention since they were found to create less resistance to the cooling fluid which results in less pumping power [40]. Velusamy and Garg [41] have studied mixed and forced convection fluid flow in ducts with elliptic and circular cross sections. They found that irrespective of the value of the Rayleigh number, the ratio of friction factor during mixed convection to corresponding value during forced convection is low in elliptical ducts compared to that in a circular duct as well as the ratio of Nusselt number to friction factor is higher for elliptic ducts compared to that for a circular duct. Despite the fact that the secondary flow in elliptical ducts is very small compare to the streamwise bulk flow, secondary motions play a significant role by cross-stream transferring momentum, heat and mass. On the hand, the main advantage of using elliptic ducts than circular ducts is the increase of heat transfer coefficient [36]. The elliptic tubes are employed in many practical fields in the area of energy conservation, design of solar collectors, heat exchangers, nuclear engineering, cooling of electrical and electronic equipment, refrigeration and air-conditioning applications, and many others. Hence, heat transfer enhancement in these devices is essential, nanofluids usage can be play effective roles to increase heat transfer coefficient.

However to the best knowledge of the authors, it is the first time which the nanofluids flow in tubes with elliptic cross section have been considered with employing two phase Mixture theory. The objective of the present paper is to study impact of nanoparticle volume fraction

(ϕ), aspect ratio and buoyancy forces on the laminar mixed convection of nanofluids flow in elliptic pipes. To aim to this purpose, laminar mixed convection Al_2O_3-water nanofluid flow in elliptic pipes with different aspect ratio (*AR*) have been investigated, employing the Brownian motions of nanoparticles for determining the thermal conductivity and dynamics viscosity of Al_2O_3-Water nanofluid, which depend on temperature. The axial velocity, secondary flow pattern, contours of temperature, distribution of nanoparticles, skin friction factor and Nusselt number profiles are presented and discussed.

2. Analysis

2.1. Mixture model

Mixed convection of a nanofluid consisting of water and Al_2O_3 nanoparticles in horizontal elliptic ducts with uniform heat flux at the solid–liquid interface has been considered. Fig. 1 shows the geometry of the considered problem. The computation domain is composed of a straight elliptic pipe with length of *L*, horizontal ellipse semi-axis of *a* and vertical ellipse semi-axis of *b*, whereas the gravitational force is exerted in the vertical direction. The channel length (*L*) is chosen 100 time of the hydraulic diameter to insure that the fully developed condition is reached at the outlet. The nanofluid flow is laminar, steady state and incompressible while dissipation and pressure work are neglected. The properties of the fluid are assumed constant except for the density in the body force, which varies linearly with the temperature (Boussinesq's hypothesis).

The mixture model, based on a single fluid two phase approach, is employed in the simulation by assuming that the coupling between phases is strong, and particles closely follow the flow. The two phases are assumed to be interpenetrating, meaning that each phase has its own velocity vector field, and within any control volume there is a volume fraction of primary

phase and also a volume fraction of the secondary phase. Instead of utilizing the governing equations of each phase separately, the continuity, momentum and fluid energy equations for the mixture are employed. Therefore, the steady state governing equations describing a mixture fluid flow and the heat transfer in elliptic pipes are as follows [30-32]:

Continuity equation:

$$\nabla \cdot \left(\rho_m V_m \right) = 0 \tag{1}$$

Momentum equation:

$$\nabla \cdot \left(\rho_m V_m V_m \right) = -\nabla p + \nabla \cdot \left(\mu_m \nabla V_m \right) + \nabla \cdot \left(\sum_{k=1}^{n} \phi_k \rho_k V_{dr,k} V_{dr,k} \right) - \rho_{m,i} \beta_m g \left(T - T_i \right) \tag{2}$$

Fluid energy equation:

$$\nabla \cdot \sum_{k=1}^{n} \left(\rho_k C_{pk} \phi_k V_k T \right) = \nabla \cdot \left(k_m \nabla T \right) \tag{3}$$

Volume fraction equation:

$$\nabla \cdot \left(\phi_p \rho_p V_m \right) = -\nabla \cdot \left(\phi_p \rho_p V_{dr,p} \right) \tag{4}$$

V_m is mass average velocity,

$$V_m = \frac{\sum_{k=1}^{n} \phi_k \rho_k V_k}{\rho_m} \tag{5}$$

In Eq. (2), $V_{dr,k}$ is the drift velocity for the secondary phase *k*, i.e. the nanoparticles in the present study,

$$V_{dr,k} = V_k - V_m \tag{6}$$

The slip velocity (relative velocity) is defined as the velocity of a secondary phase (nano particles, *p*) relative to the velocity of the primary phase (water, *f*),

$$V_{pf} = V_p - V_f \tag{7}$$

The drift velocity is related to the relative velocity,

$$V_{dr,p} = V_{pf} - \sum_{k=1}^{n} \frac{\phi_k \rho_k}{\rho_m} V_{fk} \tag{8}$$

The relative velocity is determined from Eq. (9) proposed by Manninen et al. [26] while Eq. (10) by Schiller and Naumann [33] is used to calculate the drag function f_{drag}.

$$V_{pf} = \frac{\rho_p d_p^2}{18\mu_f f_{\text{drag}}} \frac{(\rho_m - \rho_p)}{\rho_p} a^* \tag{9}$$

$$f_{\text{drag}} = \begin{cases} 1 + 0.15\text{Re}_p^{0.687} & \text{Re}_p \le 1000 \\ 0.0183\text{Re}_p & \text{Re}_p > 1000 \end{cases} \tag{10}$$

The acceleration (a^*) in Eq. (9) is:

$$a^* = \text{g} - (\text{V}_\text{m} \cdot \nabla) V_m \tag{11}$$

2.2. Nanofluid mixture properties

The employed physical properties for water-Al_2O_3 nanofluid with nanoparticle diameter of 28nm are calculated as following expressions, which the thermal conductivity and dynamic viscosity vary with temperature. The used Al_2O_3 nanoparticle and water properties for calculating the mixture properties are given in Table.1.

ρ_m is the mixture density,

$$\rho_m = (1-\phi)\rho_f + \phi\rho_p \tag{12}$$

Recently Masoumi at al. [4] have proposed an expression for predicting water-Al_2O_3 nanofluids dynamic viscosity, which is a function of temperature, mean nanoparticle diameter, nanoparticle volume fraction, nanoparticle density and the based fluid physical properties. The used expression for calculating nanofluid viscosity is given as:

$$\mu_m = \mu_f + \frac{\rho_p V_B d_p^2}{72 C \delta} \tag{13}$$

Where V_B and δ are respectively the Brownian velocity of nanoparticles and the distance between particles, which can be obtained from:

$$V_B = \frac{1}{d_p}\sqrt{\frac{18 k_B T}{\pi \rho_p d_p}} \tag{14}$$

$$\delta = \sqrt[3]{\frac{\pi}{6\phi}}\, d_p \tag{15}$$

C in Eq.(13) is defined as:

$$C = \mu_f^{-1}\left[\left(c_1 d_p + c_2\right)\phi + \left(c_3 d_p + c_4\right)\right] \tag{16}$$

Where c_1, c_2, c_3 and c_4 are given as:

$$\begin{aligned} &c_1 = -0.000\ 001\ 133, \quad c_2 = -0.000\ 002\ 771 \\ &c_3 = 0.000\ 000\ 09, \quad c_4 = -0.000\ 000\ 393 \end{aligned} \tag{17}$$

The thermal conductivity of water-Al_2O_3 nanofluid has been determined from Chon et al. [34] correlation, which considers the Brownian motion and mean diameter of the nanoparticles as follow:

$$\frac{k_m}{k_f} = 1 + 64.7\,\phi^{0.7460}\left(\frac{d_f}{d_p}\right)^{0.3690}\left(\frac{k_p}{k_f}\right)^{0.7476} \mathrm{Pr}_f^{\,0.9955}\,\mathrm{Re}_f^{\,1.2321} \tag{18}$$

Where $\mathrm{Pr_f}$ and $\mathrm{Re_f}$ in Eq. (18) are defined as:

$$\mathrm{Pr}_f = \frac{\eta}{\rho_f\, \alpha_f} \tag{19}$$

$$\mathrm{Re}_f = \frac{\rho k_B T}{3\pi\eta^2 \lambda_f} \tag{20}$$

Where λ_f is mean free path of water molecular (λ_f =0.17nm), k_B is Boltzmann constant (k_B=1.3807×10^{-23} J/K) and η has been calculated by the following equation:

$$\eta = A\cdot 10^{\frac{B}{T-C}}, \quad A=2.414\times10^{-5}, \quad B=247.8, \quad C=140 \tag{21}$$

Thermal expansion coefficient can be calculated from the presented expression by Khanafer et al. [16] as follow:

$$\beta_m = \left[\frac{1}{1+\frac{(1-\phi)\rho_f}{\phi\rho_p}} \frac{\beta_p}{\beta_f} + \frac{1}{1+\frac{\phi}{1-\phi}\frac{\rho_p}{\rho_f}} \right] \beta_f \tag{22}$$

2.3. Boundary condition

The constant heat flux boundary condition is more appropriate at the solid-fluid interface in many practical applications than the constant wall temperature, especially with laminar steady state fluid flow in heat exchangers. Therefore the constant heat flux boundary condition has been chosen for this study. Therefore, the set of coupled nonlinear differential governing equations has been solved subject to the following boundary conditions:

- At the tube inlet ($0 \le x \le a$, $0 \le y \le b$, $z = 0$): $V_{m,z} = V_i$, $V_{m,x} = V_{m,y} = 0$ *and* $T = T_i$ (23a)
- At the fluid-wall interface: ($0 \le z \le L$): $V_{m,x} = V_{m,y} = V_{m,z} = 0$ *and* $q'' = -k_m \left.\frac{\partial T}{\partial n}\right|_{wall}$ (23b)
- At the tube outlet ($0 \le x \le a$, $0 \le y \le b$, $z = L$): $p = p_0$ and an overall mass balance correction is applied.

2.4. Numerical methods

The sets of coupled non-linear differential equations were discretized using the control volume technique. A second order upwind method was used for the convective and diffusive terms while the SIMPLEC procedure was introduced to couple the velocity-pressure as described by Patankar [35]. An unstructured non uniform grid distribution has been used to discretize the computational domain as shown in Fig.2. It is finer near the tube entrance and near the wall where the velocity and temperature gradients are high. Several different grid distributions in cross section and in length direction have been tested to ensure that the calculated results are grid independent. It is shown in Fig.3 that increasing the grid numbers in

any cross section and in z direction does not change significantly the dimensionless velocity and temperature. Therefore, the grid consisted of 56×60 nodes for the present calculation has been selected in the cross section and axial direction, respectively.

After solving the governing equations for velocity, pressure, volume fraction and temperature other useful quantities such as Nusselt number and Poiseuille number can be determined.

In this paper, the Fanning friction coefficient is calculated, which is given by:

$$f = \frac{\tau_w}{\frac{1}{2}\rho_m u_i^2} \tag{24}$$

Where:

$$\tau_w = \mu_m \left.\frac{\partial u}{\partial y}\right|_w \tag{25}$$

Therefore, the local Poiseuille number (fRe) can be obtained by:

$$f\,\mathrm{Re} = 2\frac{\left.\frac{\partial u}{\partial y}\right|_w}{u_i} D_h \tag{26}$$

The local Nusselt number (Nu) can be obtained by:

$$Nu = \frac{h\,D_h}{k} \tag{27}$$

Where:

$$h = \frac{q''}{(T_w - T_b)} \tag{28}$$

After submitting Eq.(28) and Eq.(27), the local Nusselt number for the case of uniform heat flux can be calculated from:

$$Nu = \frac{q^{"} D_h}{k\left(T_w - T_b\right)} \tag{29}$$

2.5. Validations

In order to demonstrate the validity and also precision of the model assumptions and the numerical analysis, fully developed values of the Poiseuille numbers are compared with available numerical solutions for different aspect ratios from 0.25 to 1. The calculated Poiseuille numbers in Table2 show a significant agreement with numerical results by Sakalis et al. [36] and Schenk and Han [37] at different aspect ratios. The calculated fully developed Nusselt numbers are also compared with the corresponding numerical results carried out by Dunwoody [38] in an elliptic duct for different aspect ratios with uniform heat flux which is shown in Fig4a. The local Nusselt number in mixed convection is shown in Fig.4b also is compared with the experimental work of Barozzi et al. [39] in a circular tube (aspect ratio equal to 1) at Re=510, Pr=5.1 and Gr=29411. Due to comparison with single phase flow, the volume fraction solid nanoparticles are given zero (ϕ=0) for all comparisons.

For additional comparisons, the local Nusselt number and the local friction coefficient in mixed convection water-Al_2O_3 nanofluid in a straight circular tube are compared with published numerical work carried out by Mirmasoumi and Behzadmehr [32] at Re=300, Ri=1, AR=1, d_p=40 nm and ϕ=0.04. As comparisons are shown in Figure 4 and Figure 5 a significant agreement between the calculated results and reported numerical and experimental results are observed.

3. Results

Numerical simulations have been done on a wide range of Re and Ri for different values of nanoparticles concentrations and aspect ratio. However, because of similar behaviors and also due to lack of space the results presented here are for Re=300 and different Ri with three different values of nanoparticles concentrations (ϕ=0%, 2%, 5%) and four different values of aspect ratio (AR=0.25, 0.5, 0.75, 1). The effects of solid nanoparticles concentration and aspect ratio on the hydrodynamics and thermal behavior of the Al_2O_3-water nanofluids flow in elliptic pipes are presented.

3.1. Secondary flows

The secondary flows in straight elliptic heated tubes with laminar fluid flow are generated by buoyancy force, which is produced with difference between the density of fluid closed to the bottom wall and the density of fluid closed to the top wall. This gradient generates some circulation depend on fluid flow conditions. The secondary flows have a major role in heat transfer enhancement in tubes. Fig.6 shows variation of secondary flow vectors with nanoparticle volume fraction for two different Richardson numbers at fully developed region. The first row is for Ri=0.5 and the second row is for Ri=2. Two vortices appear in the elliptic heated pipe, which are symmetric with respect to the vertical plane. The secondary flows are sensitive to deviation in both the nanoparticle concentration and the buoyancy force. The secondary flow becomes stronger by increasing the nanoparticle volume fraction and the buoyancy force (increasing Ri), which could enhance heat transfer.

The secondary flow pattern changes also with deviation in the aspect ratio. Variation of the secondary flows in elliptic heated tubes with the aspect ratio is presented in Fig.7. Two vortices are also generated in the right and left part of the tube at any Ri and *AR*. It is notable

that with increasing the Richardson number two small extra vortices appear in the cross section for the case of *AR*=0.25 and Ri=1.5. Hence the buoyancy force augments with increasing Gr, an increase in the Richardson number (increasing Gr or reducing Re) strengthens the secondary flows at any aspect ratio and ϕ as illustrated in Fig6 and Fig.7.

3.2. Velocity profiles

The effects of nanoparticle concentration on the non-dimensional velocity (u/u_i) profile at the vertical semi-axis and at the axial direction are shown in Fig.8a, b and c respectively. The effects of secondary flows cause to shift the velocity profile to the bottom wall of elliptic tube; therefore symmetry with respect to the horizontal plane in the fully developed velocity profiles is disrupted. Fig.8a and 8b show that the non-dimensional fully developed velocity profile at vertical axis are not affected by the nanoparticles concentration significantly, but it is remarkable that the inlet velocity is increased with increasing ϕ to keep Re constant as illustrated in Table3. Increasing ϕ strengthens the secondary flow. Consequently, the hydraulic boundary layer is affected by the secondary flow earlier. As a result, increasing nanoparticles concentration increases velocity at centerline of the tube in the entrance length, which is shown in Fig.8c.

Variation of the velocity profile with aspect ratio for two different Ri is presented in Fig.9. The buoyancy forced does not have any significant effects at *AR*=0.25 with Ri=0.5. As a results, similar to the forced convection in a circular tube, the velocity profile in elliptic tubes with *AR*=0.25 are symmetric with respect to the horizontal plane for low Richardson number (Ri=0.5). The velocity profiles are shifted to the bottom wall of tubes with increasing aspect ratio at any Ri. It is notable that the velocity profiles are more sensitive to the aspect ratio at high Ri. Increasing aspect ratio changes the secondary flows vectors, therefore the velocity at

the center line in the entrance length changes significantly with increasing aspect ratio (see Fig.9c). It is interesting that for the case *AR*=0.25, the velocity at the center line increases continuously from the inlet value to reach the fully developed value while it has a local maximum and minimum at the entrance length for the case of higher *AR*.

3.3. Friction factor

Variation of the local friction factor with the nanoparticles concentration and the aspect ratio at Re=300 and *AR*=0.75 are illustrated in Figure 10 and Figure 11. $Z^{+}=0$ is a singular plane for the local friction factor; therefore it starts from an infinite value at the tube entrance. The friction factor decreases extremely to reach a local minimum, then the secondary flows affect the hydrodynamics boundary layer, which causes to increase the friction factor. The secondary flows increase with increasing the nanoparticles concentration (see Fig.6). The effects of secondary flows reduce the friction factor at a given Re and any Ri. Although increasing ϕ decreases the friction coefficient at any Ri, but this effect is not significant for low Ri. It is demonstrated in Fig.10b that the friction factor is affected by the secondary flows earlier for Ri=2 (about *Z*=7) when the secondary flows are strong compare to Fig.10a for Ri=0.5 (about *Z*=12).

The shape of tubes has a major effect on the friction factor. In fact, the velocity gradient at the tubes wall increases with increasing the aspect ratio. On the other hand, the secondary flows increase with increasing the aspect ratio significantly (see Fig.7). Therefore, the effects of secondary flows also decrease the friction factor. Consequently at a given Re, increasing aspect ratio decreases remarkably the friction factor in elliptic heated tubes, as it is illustrated in Fig.11. It is notable that the friction factor does not reach a local maximum at the case of *AR*=0.25 and it decreases continuously to the fully developed value at any Ri.

3.4. Contours of temperature

Contours of non-dimensional temperature ($\theta = \frac{T - T_i}{(q'' D_h)/k_m}$) for two Ri and different values of nanoparticles concentrations are shown in Fig.12. The contours of temperature are symmetry with respect to the vertical plane. Due to the vortices at secondary flows vectors, a high and low temperature zones appear at the top and bottom part of tube respectively. At a given Re and any Ri, increasing ϕ reduces the non-dimensional temperature. It is also presented in Fig.13 that increasing nanoparticle concentration decreases the non-dimensional temperature at the center line in axial direction. Consequently, the non-dimensional bulk temperature reduces with increasing ϕ.

3.5. Nanoparticles distribution

The solid nanoparticles distribution could be affected by the secondary flows pattern, which is investigated in Fig.14. Although the nanoparticles distribution is uniform and constant in the center part of tube in both vertical and horizontal direction, it varies due to the secondary flow pattern near the wall. Fig.14 clearly shows that the solid volume fraction is high at three parts of tube at a cross section, which are the bottom, right and left parts of tube, where the secondary flows are strong. On the other hand, the solid volume fraction is low at the top part of tube, where the secondary flows are weak. Consequently, the secondary flows, which are produced by the buoyancy force, change the nanoparticles distribution near the wall in horizontal elliptic tubes while it is uniform and constant at center part.

3.6. Local Nusselt number

Similar to the friction factor, $Z^+=0$ is a singular plane for the Nusselt number. Therefore, the local Nusselt number starts with an infinite value and reduces to reach a minimum. Then the secondary flows start to affect the thermal boundary layer. As a result, the local Nusselt number increases to achieve the fully developed values. Variation of the local Nusselt number with ϕ for different Ri at *AR*=0.75 is presented in Fig.15. It can be found with a comparison between Fig.15a and Fig.15b that due to the strong secondary flows at high Richardson number, the local Nusselt number augment along the tube with increasing Ri.

Increasing ϕ enhances the local Nusselt number at any Ri, but this effect is more obvious for the case of high Ri. Consequently, the nanofluids application for heat transfer enhancement is more effective in the case of high Richardson number.

It is illustrated in Fig.16 that the combination effect of the aspect ratio and the buoyancy force could increase or decrease the local Nusselt number. Increasing aspect ratio to 0.75 increases the local Nusselt number while for the case of *AR*=1, the local Nusselt number decreases, which is more significant for high Ri. It is interesting that for both Ri=0.5 and Ri=1, the elliptic tube with *AR*=0.75 and *AR*=0.25 have highest and lowest local Nusselt number, respectively.

4. Conclusions

Laminar mixed convection Al_2O_3- water nanofluid flow in elliptic tubes has been simulated to investigate effects of the aspect ratio and nanoparticles concentration on the nanofluid flow behaviors. The two phase mixture model has been employed to study the solid nanoparticles

(Al_2O_3) behaviors in the base fluid (water). The Brownian motions of nanoparticles have been considered to determine the thermal conductivity and dynamic viscosity of Al_2O_3-Water nanofluid, which depend on the temperature.

The presented results show that the secondary flows become strong with increasing the nanoparticles concentration, which augment the heat transfer coefficient. An increase in the nanoparticles volume fraction reduces the non-dimensional temperature at a given Reynolds and Richardson number. At a given Re, increasing the nanoparticles concentration increases the Nusselt number while it causes a small decrease in the friction coefficient. Increasing the aspect ratio of elliptic tubes shifts the velocity profile at the vertical semi-axis to the bottom wall of tubes. An increase in the aspect ratio reduces the skin friction factor remarkably. The Nusselt number does not have any specific behavior with increasing the aspect ratio, but it has the maximum and minimum values for the cases of AR=0.75 and AR=0.25 respectively. The elliptic tube with AR=0.75 have almost the maximum Nusselt number and the minimum friction coefficient. Therefore, the usage of the elliptic pipes with AR=0.75 instead of the circular pipe is recommended.

5. References

[1] Y.M. Xuan, Q. Li, Heat transfer enhancement of nanofluids, Int. J. Heat Fluid Flow 21 (2000) 58–64.

[2] B. X. Wang, L. P. Zhou, X. F. Peng, A fractal model for predicting the effective thermal conductivity of liquid with suspension of nanoparticles, Int. J. Heat and Mass Transfer 46 (2003) 2665–2672.

[3] H. Xie, M. Fujii, X. Zhang, Effect of interfacial nanolayer on the effective thermal conductivity of nanoparticle-fluid mixture, Int. J. Heat and Mass Transfer 48 (2005) 2926–2932.

[4] N. Masoumi, N. Sohrabi, A. Behzadmehr, A new model for calculating the effective viscosity of nanofluids, J. Phys. D: Appl. Phys. 42(2009) 055501 (6pp).

[5] C. T. Nguyen, F. Desgranges, N. Galanis, G. Roy, T. Maré, S. Boucher, H. Angue Mintsa, Viscosity data for Al_2O_3–water nanofluid—hysteresis: is heat transfer enhancement using nanofluids reliable?, Int. J. of Thermal Sciences 47(2008) 103–111.

[6] T.-P. Teng, Y.-H. Hung , T.-C. Teng , H.-E. Mo, H.-G. Hsu, The effect of alumina/water nanofluid particle size on thermal conductivity, Applied Thermal Engineering 30 (2010) 2213-2218.

[7] S.K. Das, N. Putra, P. W. Thiesen, R. Roetzel, Temperature dependence of thermal conductivity enhancement for nanofluids, J. Heat Transfer 125(2003) 567–574.

[8] N. Putra, W. Roetzel, S. K. Das, Natural convection of nanofluids, Int. J. Heat Mass Transfer 39(2003) 775–784.

[9] X. Zhang, H. Gu, M. Fujii, Effective thermal conductivity and thermal diffusivity of nanofluids containing spherical and cylindrical nanoparticles, Experimental Thermal and Fluid Science 31(2007) 593–599.

[10] N. Sankar, N. Mathew, C. B. Sobhan, Molecular dynamics modeling of thermal conductivity enhancement in metal nanoparticle suspensions, International Communications in Heat and Mass Transfer 35(2008) 867–872.

[11] W. Yu, H. Xie, L. Chen, Y. Li, Investigation of thermal conductivity and viscosity of ethylene glycol based ZnO nanofluid, Thermochimica Acta. 491(2009) 92–96.

[12] T. P. Teng, Y. H. Hung, T. C. Teng, H. E. Mo, H. G. Hsu, The effect of alumina/water nanofluid particle size on thermal conductivity, Applied Thermal Engineering 30 (2010) 2213-2218

[13] S.M.S. Murshed, K.C. Leong, C. Yang, A combined model for the effective thermal conductivity of nanofluids, Applied Thermal Engineering 29 (2009) 2477–2483

[14] S. E. Maige, C. T. Nguyen, N. Galanis, G. Roy, Heat transfer behaviors of nanofluids in a uniformly heated tube, Super Lattices Microstruct. 35 (3–6) (2004) 543–557.

[15] G. Roy, C. T. Nguyen, P.-R. Lajoie, Numerical investigation of laminar flow and heat transfer in a radial flow cooling system with the use of nanofluids, Superlattices Microstruct. 35 (3–6) (2004) 497–511.

[16] K. Khanafer, K. Vafai, M. Lightstone, Buoyancy driven heat transfer enhancement in a two dimensional enclosure utilizing nanofluids, Int. J. Heat Mass Transfer 46(2003) 3639–3653.

[17] A. Akbarinia, A. Behzadmehr, Numerical study of laminar mixed convection of a nanofluid in horizontal curved tubes, J. Apply Thermal Eng. 27(2007) 1327-1337.

[18] A. Akbarinia, Impacts of nanofluid flow on skin friction factor and Nusselt number in curved tubes with constant mass flow, Int. J. of Heat and Fluid flow 29(1) (2008) 229-241.

[19] F. Talebi, A. H. Mahmoudi, M. Shahi, Numerical study of mixed convection flows in a square lid-driven cavity utilizing nanofluid, International Communications in Heat and Mass Transfer 37(2010) 79–90.

[20] M. Shahi, A. H. Mahmoudi, F. Talebi, Numerical study of mixed convective cooling in a square cavity ventilated and partially heated from the below utilizing nanofluid, International Communications in Heat and Mass Transfer 37(2010) 201–213.

[21] L. S. Sundar, K. V. Sharma, S. Parveen, Heat transfer and friction factor analysis in a circular tube with Al_2O_3 nanofluid by using computational fluid dynamics, International Journal of Nanoparticles 2 (1-6) (2009) 191-199.

[22] V. Bianco, F. Chiacchio, O. Manca, S. Nardini, Numerical investigation of nanofluids forced convection in circular tubes, Applied Thermal Engineering 29 (2009) 3632–3642.

[23] Y. He, Y. Men, Y. Zhao, H. Lu, Y. Ding, Numerical investigation into the convective heat transfer of TiO2 nanofluids flowing through a straight tube under the laminar flow conditions, Applied Thermal Engineering 29 (2009) 1965–1972.

[24] M. Ishii, Thermo-Fluid Dynamic Theory of Two-Phase Flow, Eyrolles, Paris, 1975.

[25] C. T. Crowe, T. R. Troutt, J. N. Chung, Numerical models for two phase turbulent flows, Ann. Rev. Fluid Mech. 28(1996) 11–43.

[26] M. Manninen, V. Taivassalo, S. Kallio, On the Mixture Model for Multiphase Flow, VTT Publications 288 (1996) Technical Research Center of Finland.

[27] J. Xu, A. Rouelle, K. M. Smith, D. Celik, M. Y. Hussaini, S. W. Van Sciver, Two-phase flow of solid hydrogen particles and liquid helium, Cryogenics 44(2004) 459–466.

[28] R. Lotfi, Y. Saboohi, A. M. Rashidi, Numerical study of forced convective heat transfer of Nanofluids: Comparison of different approaches, International Communications in Heat and Mass Transfer 37(2010) 74–78.

[29] V. Bianco, O. Manca, S. Nardini, Numerical investigation on nanofluids turbulent convection heat transfer inside a circular tube, Int. J. Thermal Sciences 29(17-18)(2009) 3632-3642.

[30] A. Akbarinia, R. Laur, Investigation the Diameter of solid Particles affects on a Laminar Nanofluid Flow in a Curved Tube Using a Two Phase Approach, Int. J. Heat fluid flow 30 (4)(2009) 706-714.

[31] S. Mirmasoumi, A. Behzadmehr, Numerical study of laminar mixed convection of a nanofluid in a horizontal tube using two-phase mixture model, Applied Thermal Engineering 28(2008) 717–727.

[32] S. Mirmasoumi, A. Behzadmehr, Effect of nanoparticles mean diameter on mixed convection heat transfer of a nanofluid in a horizontal tube, International Journal of Heat and Fluid Flow 29(2008) 557–566.

[33] L. Schiller, A. Naumann, A drag coefficient correlation, Z. Ver. Deutsch. Ing. 77(1935) 318–320.

[34] C. H. Chon, K. D. Kihm, S. P Lee, S. U. S Choi, Empirical correlation finding the role of temperature and particle size for nanofluid (Al_2O_3) thermal conductivity enhancement, J. Applied Physic 87 (5)(2005) 153107 (3pages).

[35] S.V. Patankar, Numerical Heat Transfer and Fluid Flow, Hemisphere, Washington, 1980.

[36] V. D. Sakalis, P. M. Hatzikonstaninoi, N., kafousias, Thermally developing flow in elliptic ducts with axially variable wall temperature distribution, International Journal of Heat and Mass Transfer 45(2002) 25-35.

[37] J. Schenk, B. S. Han, Heat transfer from laminar flow in ducts with elliptic cross section, Appl. Sci. Res. 17(1966) 96-114.

[38] N. T., Dunwoody, Thermal results for forced convection through elliptical ducts, J. Appl. Mech. 29 (1962) 165-170.

[39] G. S. Barozzi, E. Zanchini, M. Mariotti, Experimental investigation of combined forced and free convection in horizontal and inclined tubes, Meccanica 20(1) (1985) 18-27.

[40] K. Velusamy, V. K. Garg, G. Vailyanathan, Fully developed flow and heat transfer in semi-elliptical ducts, Int. J. Heat and Fluid flow 16 (1995) 145-152.

[41] K. Velusamy and V. K. Garg, Laminar mixed convection in vertical elliptic ducts, Int. J. Heat Mass Transfer 39 (4) (1996) 745-752.

List of Tables

Table 1.Thermophysical properties of nanoparticles and base fluid at 27^0C.

Table2. Comparison of the Poiseuille number at fully developed region with previous numerical results.

Table3. Variation of the inlet velocity and nanofluid properties with the nanoparticle volume fraction at Re=300.

List of Figures

Figure1. Problem geometry and coordinate system for an elliptic duct.

Figure2. Unstructured non-uniform used grid for an elliptic duct.

Figure3. Grid independent test column a)in any cross section and column b) in axial direction.

Figure4. Comparison of the Nusselt number with a) fully developed Nusselt number carried by Dunwoody [38] b) local Nusselt number values carried by Barozzi et al. [39].

Figure5. Comparison of the local Nusselt number and the local friction factor with previous numerical results carried by Mirmasoumi and Behzadmehr [32] at Re=300, Ri=1, AR=1, d_p=10nm and ϕ=0.02.

Figure6. The secondary flow vectors at fully developed region for different ϕ at AR=0.75, a) Ri=0.5 and b) Ri=2.

Figure7. The secondary flow vectors for different aspect ratio at ϕ=0.05, Re=300 and a) Ri=0.5 and b) Ri=1.5.

Figure8. Variation of non-dimensional velocity profile with ϕ at Re=300, Ar=0.75, d_p=28nm in fully developed zone at vertical ellipse semi-axis for Ri=0.5 (a) and Ri=2 (b) and at center line in axial direction for Ri=1(c).

Figure9. The non-dimensional velocity profile for different AR at Re=300, d_p=28nm and ϕ=0.05 in fully developed zone at vertical ellipse semi-axis for Ri=0.5(a) and Ri=1.5 (b) and at center line in axial direction for Ri=1 (c).

Figure10. Variation of the friction factor with ϕ at Re=300, AR=0.75 and d_p=28nm for a) Ri=0.5 and b) Ri=2.

Figure11. Variation of the friction factor with aspect ratio at Re=300, ϕ=0.05 and d_p=28nm for a) Ri=0.5 and b) Ri=1.5.

Figure12. Contours of the non-dimensional temperature at fully developed region for different ϕ at AR=0.75, Re=300, at a) Ri=0.5 and b) Ri=2.

Figure13. The non-dimensional temperature profiles for different ϕ at center line in axial direction for Re=300, Ri=1, AR=0.75 and d_p=28nm.

Figure14. Variation of the solid nanoparticle distribution with Richardson number at Re=300, AR=0.75, ϕ=0.05 and d_p=28nm at a) vertical ellipse semi-axis and b) horizontal ellipse semi-axis.

Figure15. Variation of the local Nusselt number with solid nanoparticles volume fraction at Re=300, AR=0.75 and d_p=28nm for a) Ri=0.5 and b) Ri=2.

Figure16. Variation of the local Nusselt number with aspect ratio at Re=300, ϕ=0.05 and d_p=28nm for a) Ri=0.5 and b) Ri=1.5.

Elsevier reference: **ATE 3490**
Editorial reference: **ATE_ATE-2010-890**
Applied Thermal Engineering
Title: **Numerical Study of Two Phase Laminar Mixed Convection Nanofluid in Elliptic Ducts**

Dear Sir/Madam
Thank you for your consideration. The research highlights of the accepted paper are as follows:

Research highlights

1. The nanofluid flow is simulated using the two phase mixture model.
2. The Brownian motions and the dependence on temperature are considered.
3. At a given Re, the nanofluids utilization in elliptic duct can enhances heat transfer.
4. Using the elliptic pipes with AR=0.75 have more advantages than the circular pipes.
5. The elliptic ducts with AR=0.75 have the maximum Nusselt number.

With the best regards

Alireza Akbarinia
Corresponding author

Alireza Akbarinia
University of Bremen
Bremen, Germany
Email: a.akbarinia@item.uni-bremen.de
Tel(w):+49 421 21862517
Mobile: +49 176 82068078

Table 1.

Thermophysical properties of nanoparticles and base fluid at 20^0C

Properties	Water	Nanoparticle(Al_2O_3)
Density $\boldsymbol{\rho}$(kg/m^3)	998.2	3720
Heat capacity $\mathbf{C_p}$ (J/kg.K)	4182	880
Thermal conductivity **k** (W/mK)	0.6028	35

Table2.
Comparison of the Poiseuille number at fully developed region with previous numerical results.

AR=b/*a*	$(f\,\mathrm{Re})_{fd}$		
	Previous numerical results (Sakalis et al., [36])	Previous numerical results (Schenk and Han, [37])	Present calculation
0.25	18.258	18.29	18.36
0.5	16.896	16.823	16.85
0.75	16.255	16.317	16.25
1	16.02	16	16.03

Table 3.

Variation of the inlet velocity and nanofluid properties with the nanoparticle volume fraction at Re=300.

ϕ	Inlet velocity V_i (m/s)	Dynamic viscosity μ_m (N s/m)	Thermal conductivity k_m (W/mK)	Density ρ (kg/m^3)
0	0.0302826	0.0010074	0.6028	998
0.02	0.0339028	0.0011893547	0.6376101	1052.4
0.05	0.0499868	0.0018896	0.6717555	1134.1

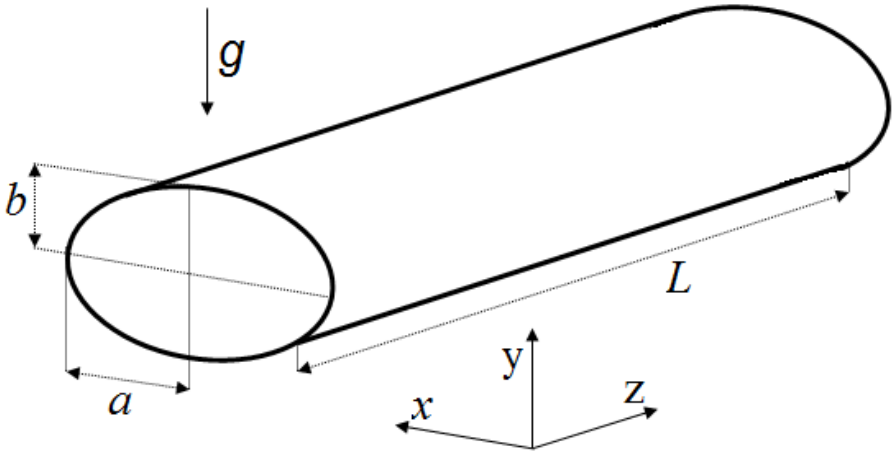

Fig.1 Problem geometry and coordinate system for an elliptic duct.

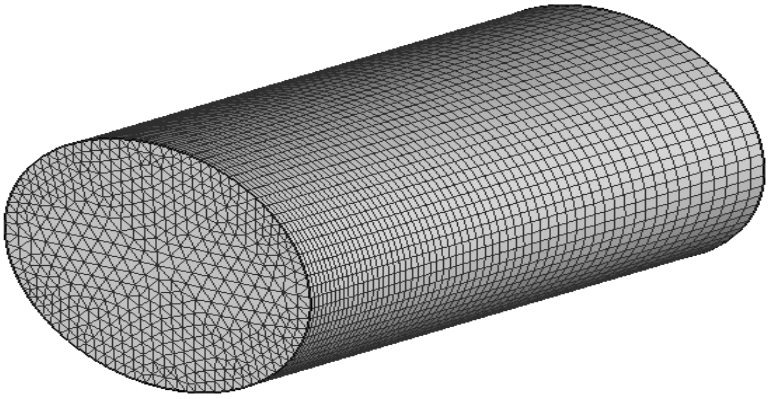

Fig.2 Unstructured non-uniform used grid for an elliptic duct.

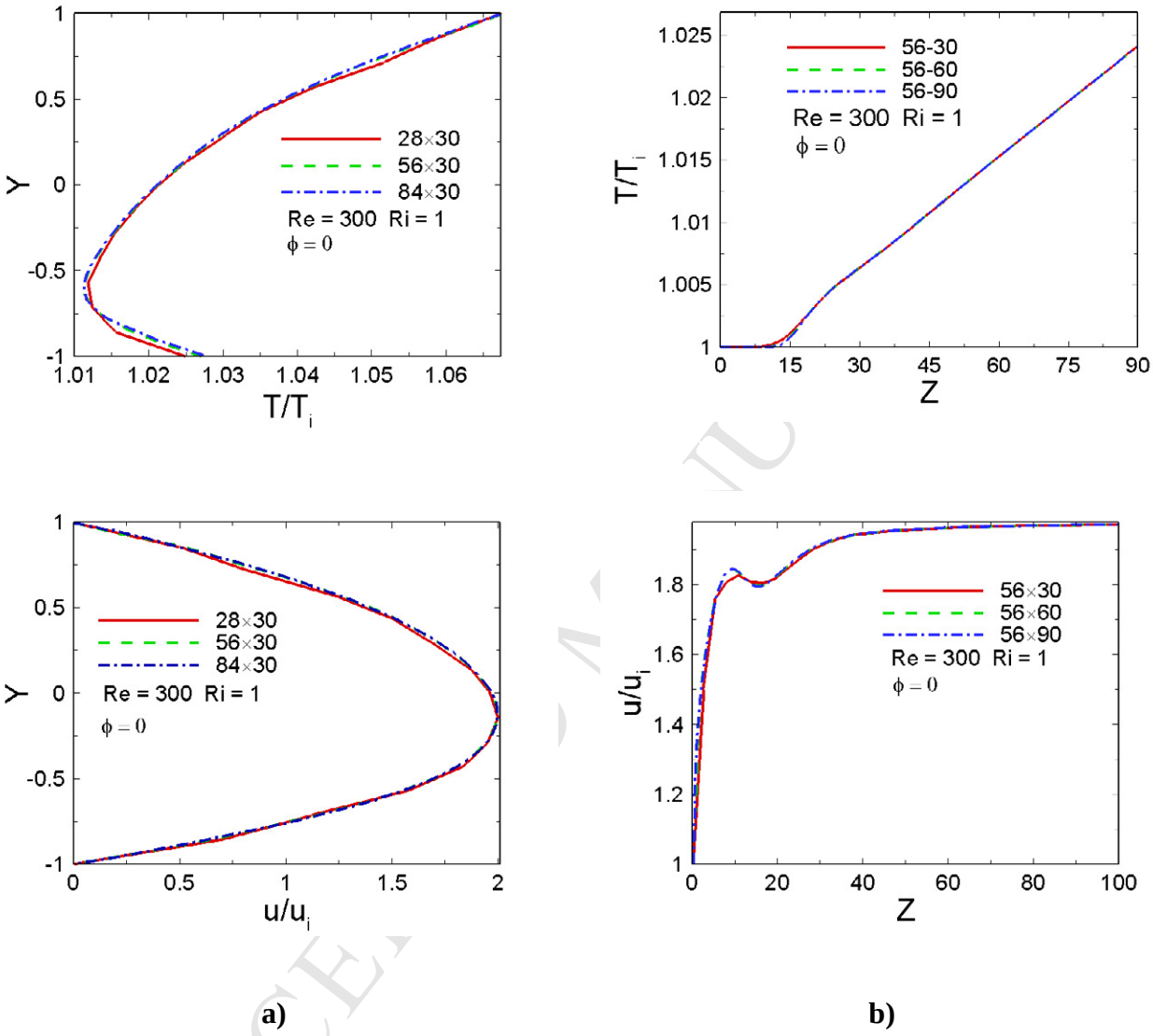

a) **b)**

Fig.3 Grid independent test column a) in any cross section and column b) in axial direction.

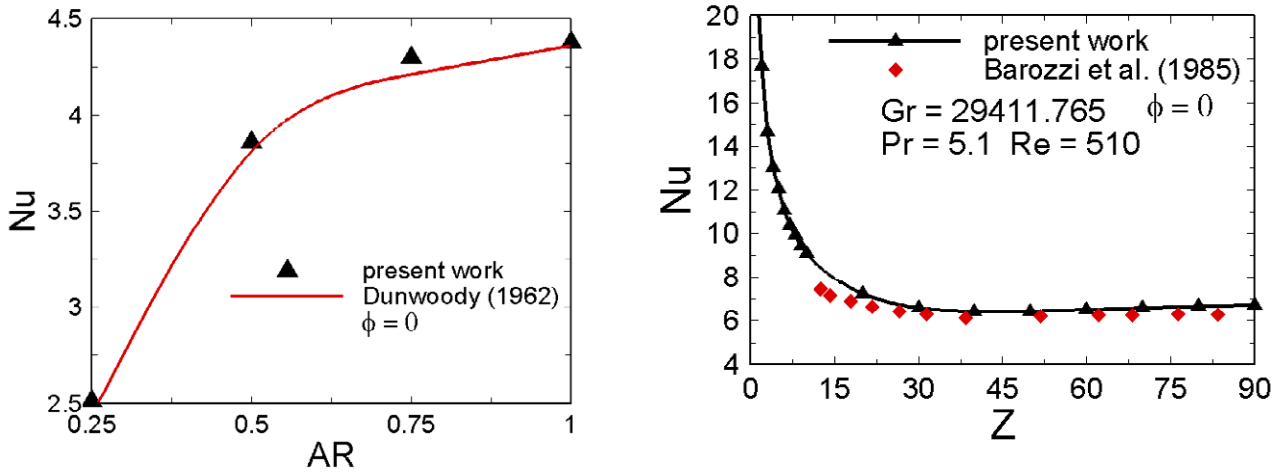

a) **b)**

Fig.4. Comparison of the Nusselt number with a) fully developed Nusselt number carried by Dunwoody [38] b) local Nusselt number values carried by Barozzi et al. [39].

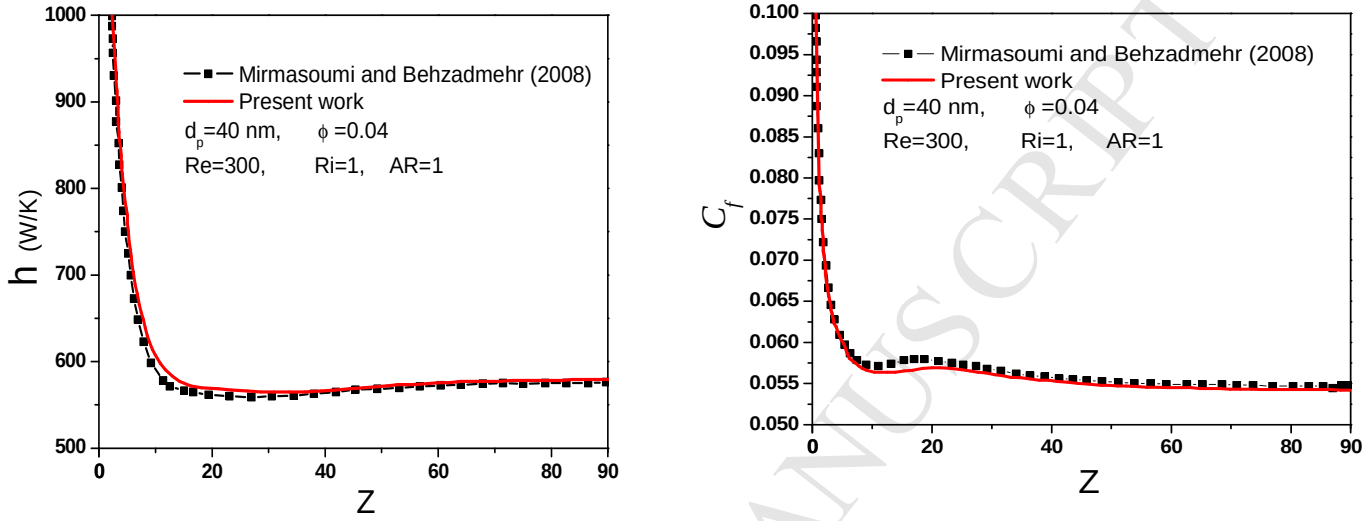

Fig.5. Comparison of the local Nusselt number and the local friction factor with previous numerical results carried by Mirmasoumi and Behzadmehr [32] at Re=300, Ri=1, AR=1, d_p=40nm and ϕ=0.04.

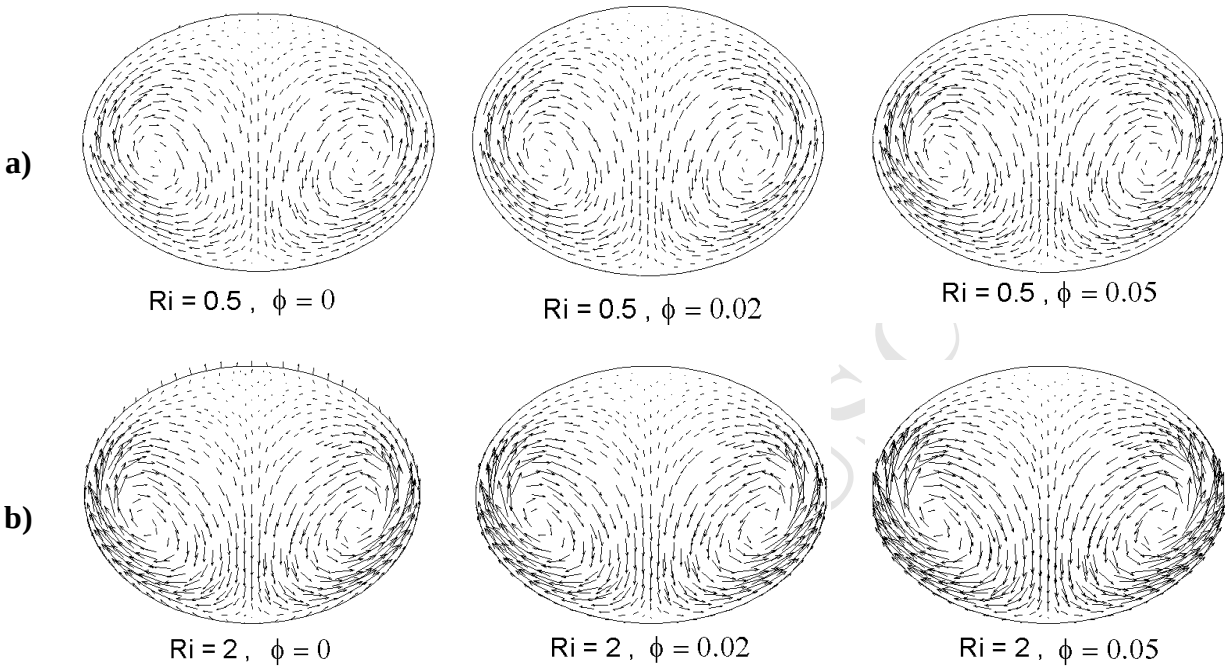

Fig.6 The secondary flow vectors at fully developed region for different ϕ at AR=0.75, a) Ri=0.5 and b) Ri=2.

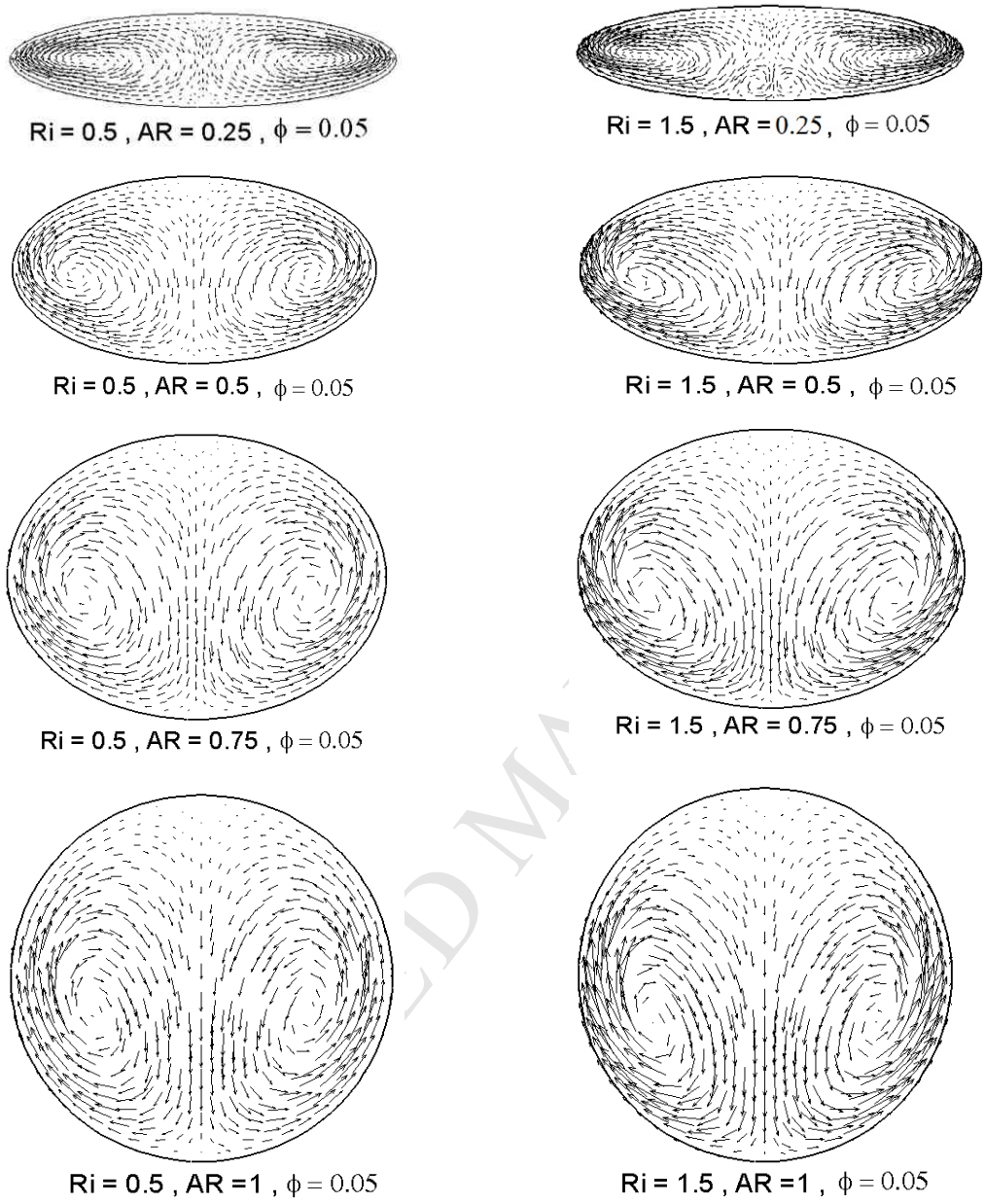

Fig.7 The secondary flow vectors for different aspect ratio at ϕ=0.05, Re=300 and a) Ri=0.5 and b) Ri=1.5.

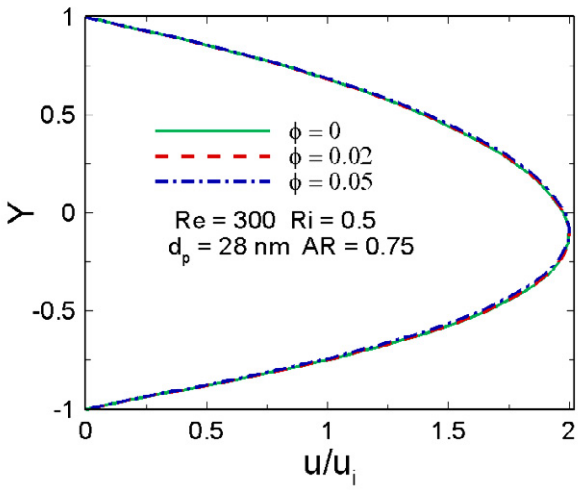

a)

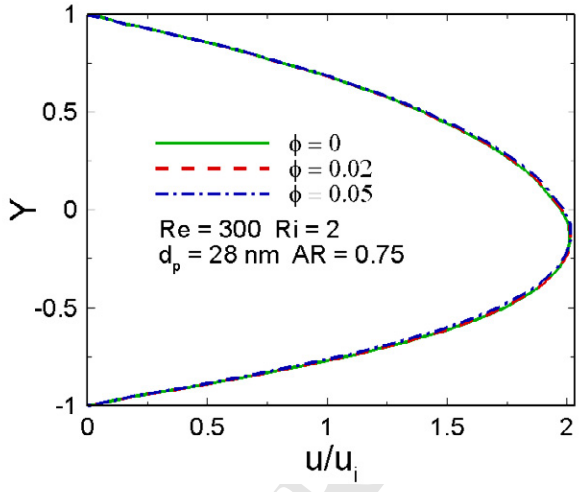

b)

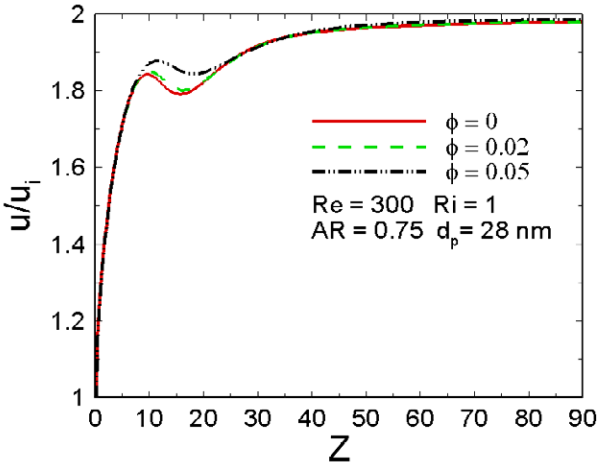

c)

Fig.8 Variation of non-dimensional velocity profile with ϕ at Re=300, *Ar*=0.75, d_p=28nm in fully developed zone at vertical ellipse semi-axis for Ri=0.5 (a) and Ri=2 (b) and at center line in axial direction for Ri=1(c).

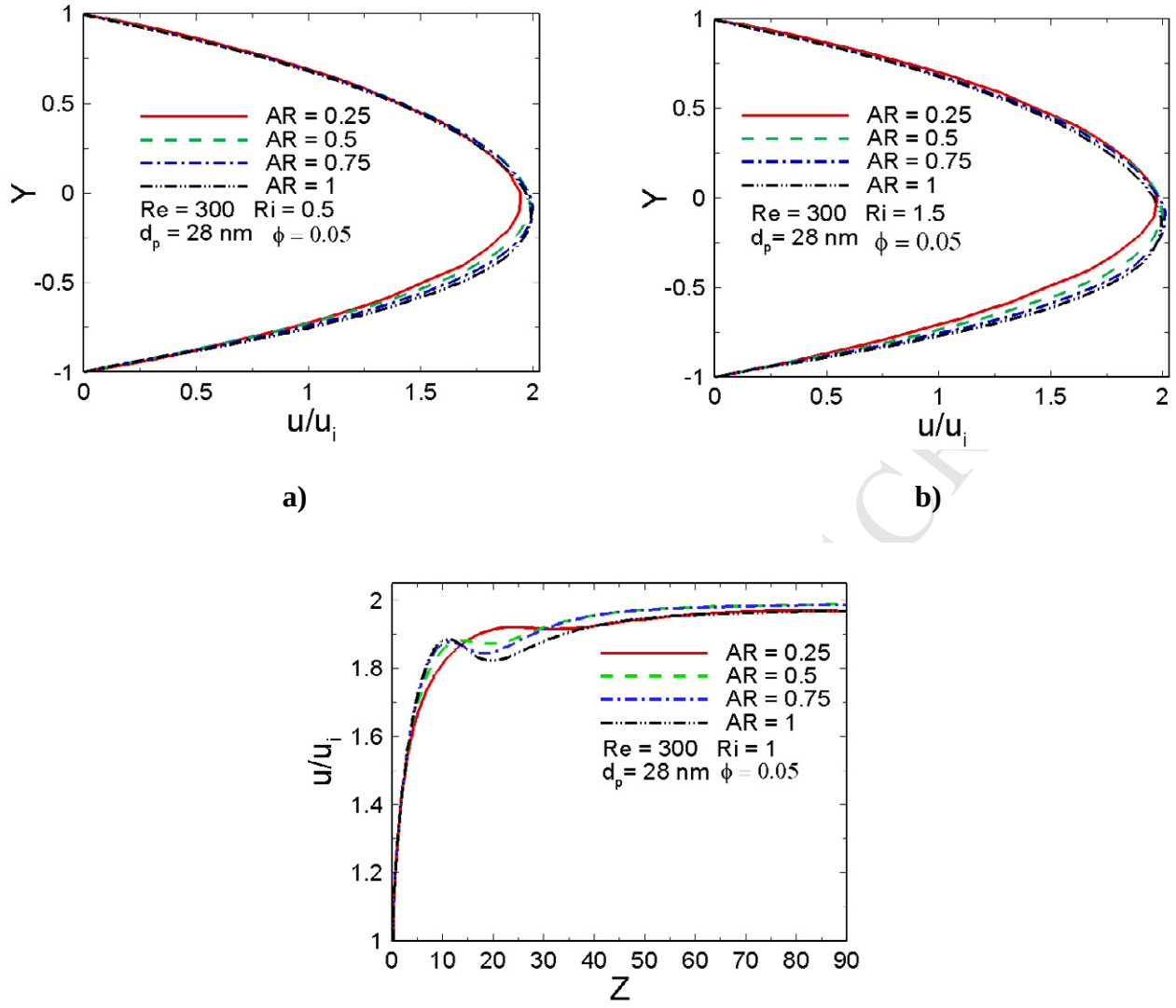

Fig. 9 The non-dimensional velocity profile for different *AR* at Re=300, d_p=28nm and ϕ=0.05 in fully developed zone at vertical ellipse semi-axis for Ri=0.5(a) and Ri=1.5 (b) and at center line in axial direction for Ri=1 (c).

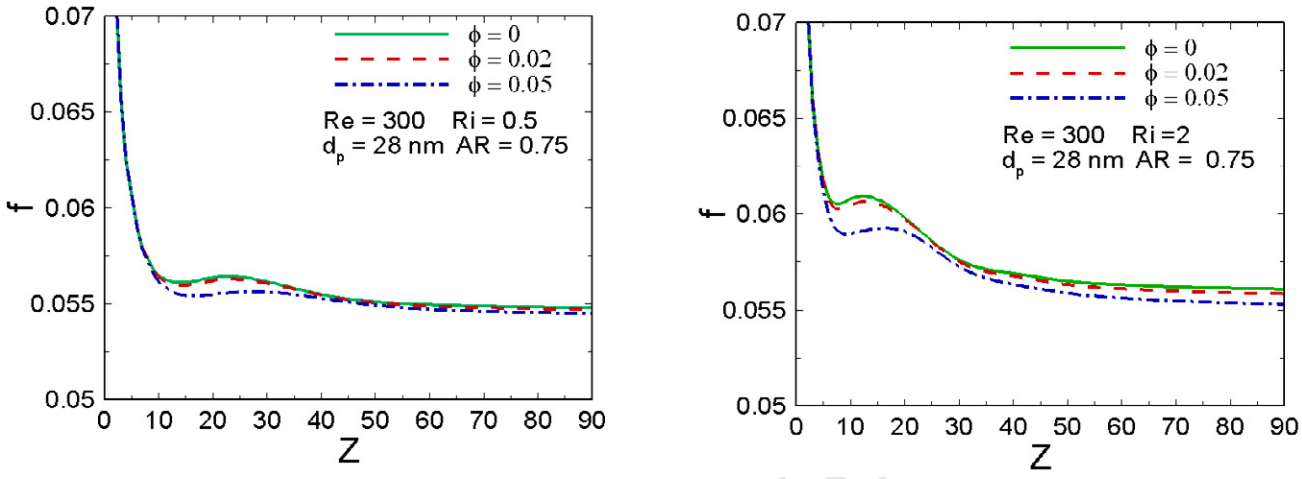

a) **b)**

Fig.10 Variation of the friction factor with ϕ at Re=300, *AR*=0.75 and d_p=28nm for a) Ri=0.5 and b) Ri=2.

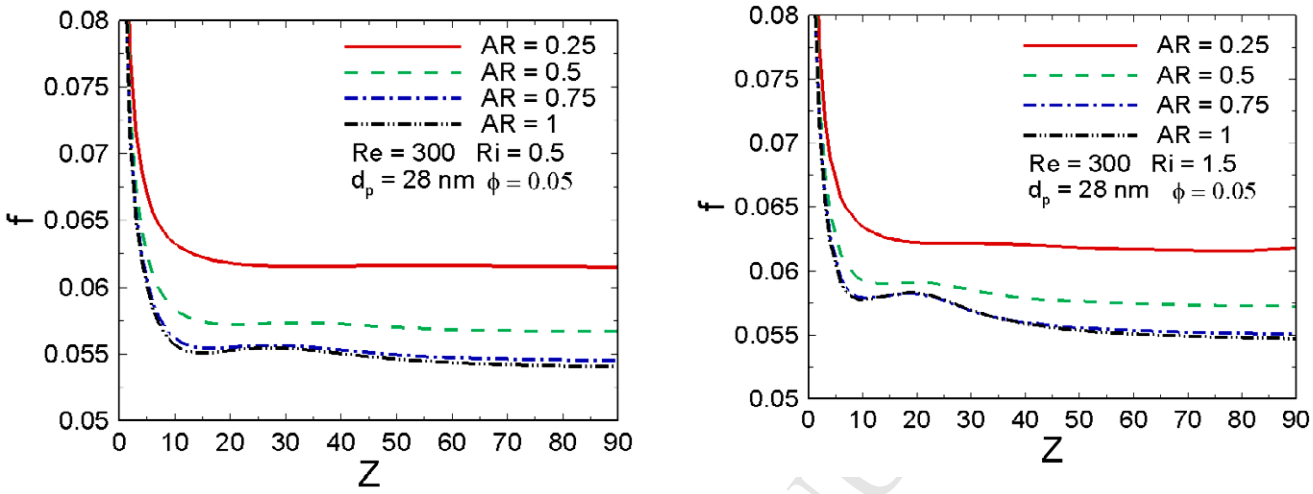

Fig.11 Variation of the friction factor with aspect ratio at Re=300, ϕ=0.05 and d_p=28nm for a) Ri=0.5 and b) Ri=1.5.

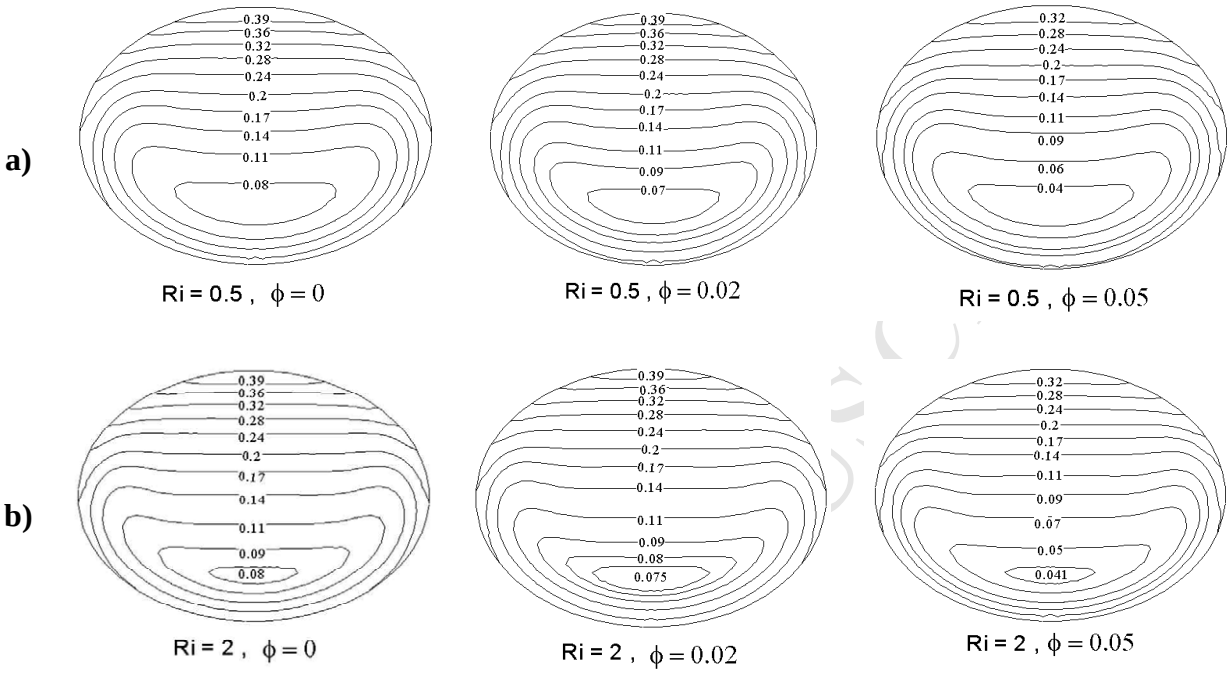

Fig.12 Contours of the non-dimensional temperature at fully developed region for different ϕ at *AR*=0.75, Re=300, at a) Ri=0.5 and b) Ri=2.

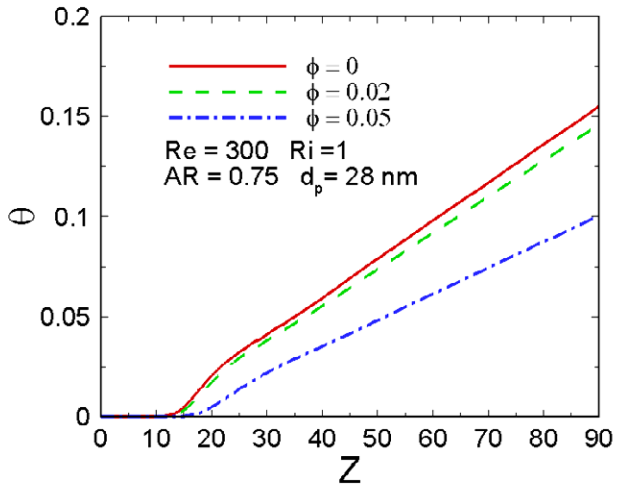

Fig.13 The non-dimensional temperature profiles for different ϕ at center line in axial direction for Re=300, Ri=1, *AR*=0.75 and d_p=28nm.

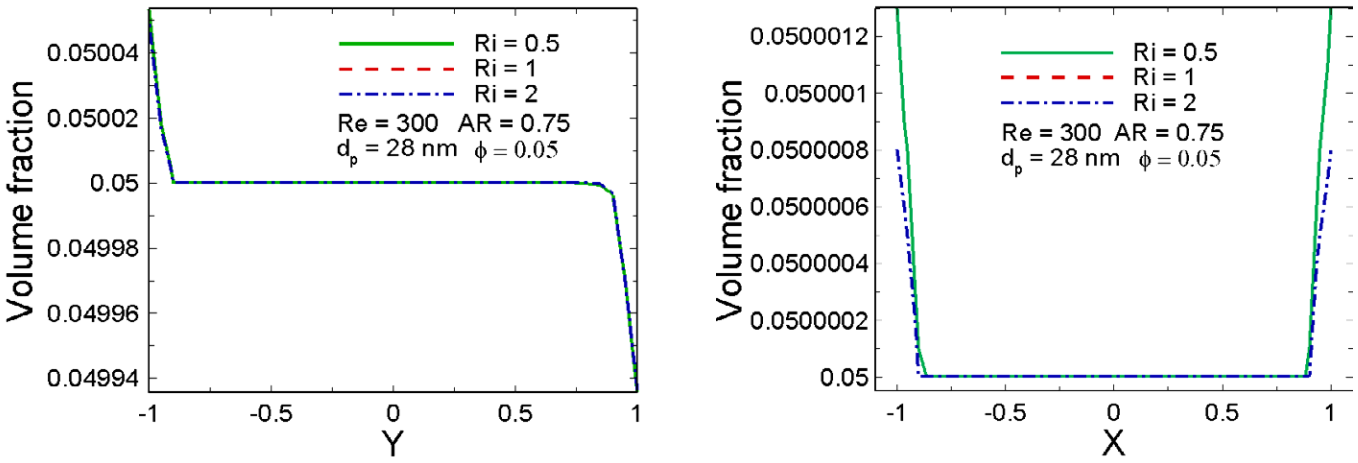

a) **b)**

Fig.14 Variation of the solid nanoparticle distribution with Richardson number at Re=300, *AR*=0.75, ϕ=0.05 and d_p=28nm at a) vertical ellipse semi-axis and b) horizontal ellipse semi-axis.

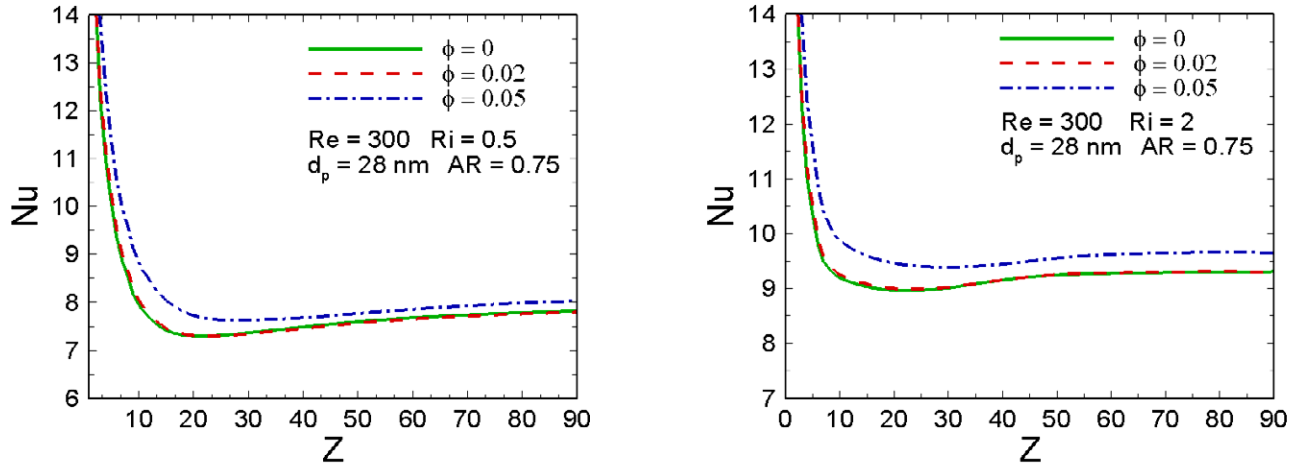

a) **b)**

Fig.15 Variation of the local Nusselt number with solid nanoparticles volume fraction at Re=300, *AR*=0.75 and d_p=28nm for a) Ri=0.5 and b) Ri=2.

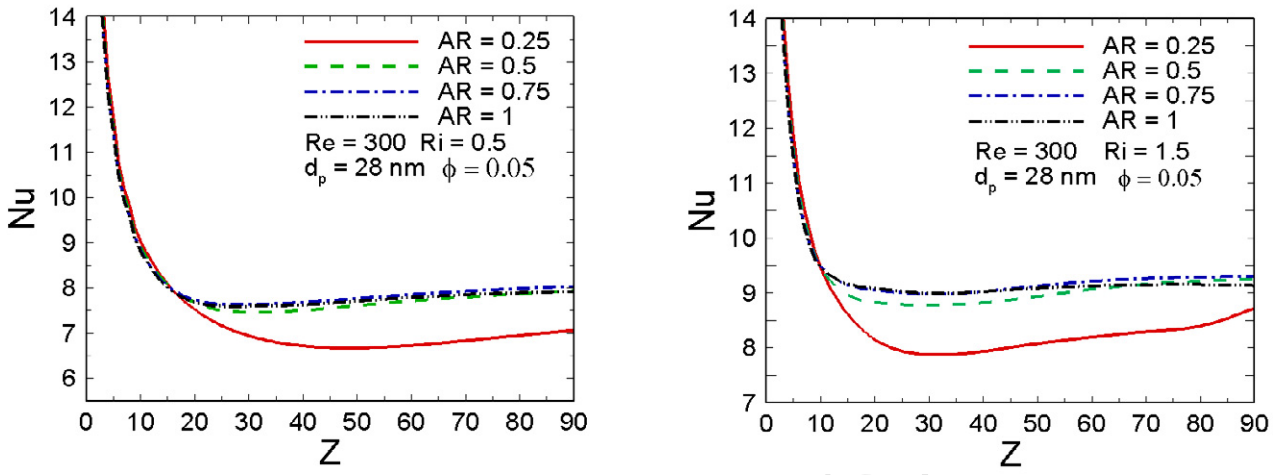

a) **b)**

Fig.16 Variation of the local Nusselt number with aspect ratio at Re=300, ϕ=0.05 and d_p=28nm for a) Ri=0.5 and b) Ri=1.5.